Meteoritics & Planetary Science 60, Nr 10, 2458-2468 (2025) doi: 10.1111/maps.70046

Century-scale effect of climate change on meteorite falls

Elov PEÑA-ASENSIO 10,1,2*. Denis VIDA,3,4. Ingrid CNOSSEN,5, and Esteban FERRER

¹Department of Aerospace Science and Technology, Politecnico di Milano, Milan, Italy ²ETSIAE-UPM-School of Aeronautics, Universidad Politécnica de Madrid, Madrid, Spain ³Department of Physics and Astronomy, University of Western Ontario, London, Ontario, Canada ⁴Institute for Earth and Space Exploration, University of Western Ontario, London, Ontario, Canada ⁵British Antarctic Survey, Cambridge, UK

*Correspondence

Eloy Peña-Asensio, Department of Aerospace Science and Technology, Politecnico di Milano, Via La Masa 34, 20156 Milan, Italy.

Email: eloy.pena@polimi.it, eloy.peas@gmail.com

(Received 30 March 2025; revision accepted 25 August 2025)

Abstract-Climate change is inducing a global atmospheric contraction above the tropopause $(\sim 10 \text{ km})$, leading to systematic decrease in neutral air density. The impact of climate change on small meteoroids has already been observed over the last two decades, with documented shifts in their ablation altitudes in the mesosphere (~50-85 km) and lower thermosphere $(\sim 85-120 \text{ km})$. This study evaluates the potential effect of these changes on meteorite-dropping fireballs, which typically penetrate the stratosphere ($\sim 10-50$ km). As a case study, we simulate the atmospheric entry of the fragile Winchcombe carbonaceous chondrite under projected atmospheric conditions for the year 2100 assuming a moderate future emission scenario. Using a semi-empirical fragmentation and ablation model, we compare the meteoroid's light curve and deceleration under present and future atmospheric density profiles. The results indicate a modest variation of the ablation heights, with the catastrophic fragmentation occurring 300 m lower and the luminous flight terminating 190 m higher. The absolute magnitude peak remains unchanged, but the fireball would appear 0.5 dimmer above ∼120 km. The surviving meteorite mass is reduced by only 0.1 g. Our findings indicate that century-scale variations in atmospheric density caused by climate change moderately influence bright fireballs and have a minimal impact on meteorite survival.

INTRODUCTION

The increase in atmospheric CO₂ concentration causes net warming in the troposphere ($\sim 0-10 \text{ km}$), but results in cooling from the stratosphere (\sim 10–50 km) upward (Manabe & Wetherald, 1967, 1975; Roble & Dickinson, 1989). This has widespread effects on the climate of the stratosphere (\sim 10–50 km), mesosphere $(\sim 50-85 \text{ km})$, and thermosphere $(\sim 85-500 \text{ km})$, including thermal contraction: cooling of the middle and upper atmosphere causes this part of the atmosphere to shrink, so that the atmospheric mass density at high altitudes shows a multi-decadal decrease (e.g., Cnossen et al., 2024; Emmert, 2015; Weng et al., 2020). This has important practical consequences for the lifetime of space debris in low Earth orbit and long-term satellite mission planning (e.g., Brown et al., 2021, 2024).

At lower altitudes, between the mesosphere and the lower thermosphere, atmospheric contraction has also significantly affected meteor ablation altitudes—the height at which a small space rock (meteoroid) enters the atmosphere and produces visible radiation due to its interaction with the air (Koschny & Borovicka, 2017). A thinning upper atmosphere should, in principle, lead to a systematic lowering of meteor ablation height, as the altitude at which meteoroids ablate depends on atmospheric mass density.

Observational studies using radars have consistently documented such trends in small impacting meteoroids (magnitude +8 and fainter; roughly 100-2000 µm in diameter), providing empirical evidence that the shrinking atmosphere is altering the height distribution of meteors detected by ground-based systems. Early observations by Clemesha and Batista (2006) revealed fluctuations in meteor centroid altitudes in Cachoeira Paulista, Brazil (23°S, 45°W), with reported decreases ranging from 300 to 800 m per decade between 2000 and 2005. Jacobi (2014) examined meteor altitudes at Collm, Germany (51.3° N, 13.0° E) and reported a trend of -560 m per decade, with an additional solar cycle effect of +450 m per 100 solar flux units, indicating that both cooling and solar activity modulate the observed altitudes. Similarly, Lima et al. (2015) observed a comparable decrease of 380 m per decade in Cachoeira Paulista, Brazil, after accounting for solar variability. More recently, a data set from Tirupati, India (13.63° N, 79.4° E) showed a decrease of 228 m per decade in meteor peak altitude over an 11-year period (Venkat Ratnam et al., 2025).

The sensitivity of meteor ablation to atmospheric density fluctuations is further demonstrated by the response of meteor peak flux altitudes to planetary wave activity. Stober et al. (2012) showed that large-scale atmospheric perturbations can cause measurable shifts in meteor heights from 4 months of observations made in Collm, Juliusruh, Germany (54.6° N, 13.4° E), and Andenes, Norway (69.3° N, 16.0° E). Extending these findings to longer timescales, Stober et al. (2014) used a decade of meteor radar observations from the Canadian Meteor Orbit Radar (CMOR) in Ontario, Canada (43.3° N, 80.8° W), to estimate changes in neutral air density and reported a decrease of 5.8% per decade at approximately 91 km altitude, consistent with expectations from global climate models.

Recent large-scale analyses provide further confirmation that this trend is not limited to specific locations. Using over 20 years of data from 12 meteor radars distributed over a broad range of latitudes, Dawkins et al. (2023) reported that meteor ablation altitudes are decreasing at all sites, with trends ranging from 10 to 818 m per decade. This study also found a strong correlation between meteor heights and solar activity at most stations, but confirmed that multi-decadal mesospheric cooling due to increasing greenhouse gas concentrations is systematically lowering the altitude at which meteors are detected.

Although these studies primarily focus on small meteoroids detected by radar, similar mechanisms may apply to larger objects, including meteorite-dropping bright meteors (or fireballs), as the atmospheric density profile can have significant effects on meteorite survival

dynamical modeling (Lyytinen & Gritsevich, 2016). A reduction in atmospheric density could alter the depth at which fireballs begin and end their luminous phase, potentially affecting the likelihood of meteorite survival. It is therefore conceivable that climate change in the entire atmosphere could affect the meteorite fall rate as well, especially of fragile carbonaceous chondrites, which require specific conditions to survive atmospheric flight (Brown et al., 2002). The purpose of this study is to investigate this further, using the Winchcombe carbonaceous chondrite meteorite (Gattacceca et al., 2022) fall as a case study.

The remainder of the paper is organized as follows. We first detail the methodology in "Methods" section to then present and discuss the results in "Results" section. Finally, conclusions can be found in "Conclusions" section.

METHODS

This section outlines the methodology used to assess the potential effects of atmospheric density variations on meteorite-dropping fireballs, using the Winchcombe meteorite fall as a case study. First, we describe the observational data and key physical characteristics of the Winchcombe meteorite fall (The Winchcombe meteorite section), which serve as the foundation for the subsequent modeling. Next, we detail the fragmentation and erosion model applied to reproduce the observed meteoroid's atmospheric entry (Meteoroid Atmospheric Entry Model section). Then we present the methodology used to estimate century-scale trends in atmospheric density based on climate change simulations (Atmospheric Density Projection section). Finally, we use these predictions to simulate the Winchcombe fireball under different atmospheric conditions, allowing us to evaluate possible modifications in its luminous trajectory and meteorite survival (Simulating Winchcombe Fall With Another Atmosphere Density Profile section).

The Winchcombe Meteorite

The Winchcombe meteorite fall on February 28, 2021, in the United Kingdom, represents one of the best-documented cases of a fireball with recovered meteorites (King et al., 2022; McMullan et al., 2024; Russell et al., 2024; Suttle et al., 2024). The fireball was recorded by 16 optical stations, including dedicated meteor camera networks and casual video recordings, providing accurate measurements of atmospheric trajectory, fireball dynamics, light curve, and fragmentation. The event was observed by multiple fireball networks, including the UK Fireball Network (UKFN) within the Global Fireball Observatory (GFO, Devillepoix et al., 2020), the System

for Capture of Asteroid and Meteorite Paths (SCAMP) within the French Fireball Recovery and InterPlanetary Observation Network (FRIPON, Colas et al., 2020), the Global Meteor Network (GMN, Vida, Šegon, et al., 2021), the UK Meteor Observation Network (UKMON, Campbell-Burns & Kacerek, 2014), the Network for Meteor Triangulation and Orbit Determination (NEMETODE, Stewart et al., 2013), and the AllSky7 network (Hankey et al., 2020), with the UK Fireball Alliance (UKFAll, Daly et al., 2020) coordinating the efforts in the UK.

The progenitor meteoroid had a very small estimated initial mass of approximately 13 kg and entered Earth's atmosphere with a relatively low velocity of 13.9 km/s. The fireball was first detected at an altitude of 90.6 km and remained observable down to 27.6 km, where its velocity dropped to approximately 3 km/s (McMullan et al., 2024). The meteoroid experienced a major fragmentation event at 35 km altitude, producing multiple trackable fragments.

Winchcombe is classified as a CM2 carbonaceous chondrite, a rare and fragile meteorite type with a high volatile and water content. The meteorite has a bulk density of approximately 2090 kg/m³, consistent with micro-X-ray computed tomography measurements of recovered fragments (King et al., 2022). The total recovered mass from the strewn field was approximately 0.6 kg, with the largest fragment weighing 0.319 kg.

Winchcombe is an ideal case study for atmospheric effects on meteoroid survival, not only due to its high-quality observational data but also its fragility. While C-type asteroids comprise 13-20% of near-Earth objects (Binzel et al., 2019; Hromakina et al., 2021; Ieva et al., 2020), carbonaceous chondrites make up only $\sim 4\%$ of recovered meteorites¹, indicating most disintegrate during entry. Dynamical modeling suggests that carbonaceous materials may constitute over 50% of the terrestrial impactor population (Brož et al., 2024), further reinforcing this survival bias. Their extreme weakness some, like Tagish Lake, crumble by hand (Brown et al., 2000)—makes them particularly susceptible to both thermal fragmentation in space and atmospheric filtering during entry (Shober et al., 2025). If climate change influences meteoroid fragmentation and ablation, carbonaceous chondrites would be the first to reveal these effects.

Meteoroid Atmospheric Entry Model

The atmospheric entry of the meteoroid was analyzed using a semi-empirical ablation model developed by Borovička et al. (2013), following the manual modeling procedure detailed in Borovička et al. (2020) and using the implementation by Vida et al. (2023).

The initial meteoroid is modeled as a classical single body that fragments at manually determined points. The physical parameters of the initial meteoroid and individual fragments are also manually estimated. The fragmentation points are informed by brightness increases in the light curve (i.e., flares) and a consequent increase in the observed deceleration. Most fragmentations were modeled as the release of an eroding fragment (see Borovička, Spurný, and Brown (2015) for more details), which is a body that rapidly erodes by the release of mm-sized grains. The grain masses are distributed according to a power law (a differential mass index of s = 2.0 is assumed) within a given range of masses. The amount of erosion is regulated by the erosion coefficient η , which determines how much mass is eroded from the fragment per unit of kinetic energy loss. Both the main body and fragmented grains are modeled using the classical single-body ablation equations (Ceplecha et al., 1998):

$$\frac{dv}{dt} = -Km^{-1/3}\rho_{\text{air}}v^2,\tag{1}$$

$$\frac{dm_a}{dt} = -K\sigma m^{2/3} \rho_{\rm air} v^3,\tag{2}$$

where K is the shape density coefficient, m is the meteoroid mass (m_a is the ablated mass), v is the velocity, and $\rho_{\rm air}$ is the atmospheric density taken from the NRLMSISE-00 model (Picone et al., 2002). The ablation coefficient, σ , represents the fraction of the kinetic energy converted into mass loss. As the density and shape of the meteoroid cannot be measured independently, the coefficient K is defined as:

$$K = \frac{\Gamma A}{\rho_{n_0}^{2/3}},\tag{3}$$

where Γ is the drag coefficient (typically set at 1), A is the shape factor (taken as 1.21 for spheres), and ρ_m is the bulk density of the meteoroid or individual grains.

The equations of motion and ablation were numerically integrated using a fourth-order Runge–Kutta scheme with a time step of 2 ms. The integration of individual fragments was stopped if the mass of the fragment fell below 10⁻¹⁴ kg or if the velocity dropped below 2.5 km/s, the assumed ablation limit (Ceplecha et al., 1998).

The total luminosity generated by ablation is computed as:

$$I = -\tau \frac{v^2}{2} \frac{dm_a}{dt} + mv \frac{dv}{dt},\tag{4}$$

where τ is the luminous efficiency. The luminous efficiency function used in this work followed the formulation given by Borovička et al. (2020).

For cases where the body or its fragments undergo erosion, the mass loss due to erosion follows a formulation similar to that of ablation:

$$\frac{dm_e}{dt} = -K\eta m^{2/3} \rho_{\rm air} v^3,\tag{5}$$

where η is the erosion coefficient. The eroded mass is distributed into smaller fragments whose masses follow a power law distribution defined by the mass index s and the range of ejected masses. These fragments ablate independently and single-body equations are integrated for each, with the total fireball luminosity being the sum of luminosities of all ablating fragments at a given time.

The total mass loss for an object in the simulation at any given time is the sum of ablation and erosion contributions:

$$\frac{dm}{dt} = \frac{dm_a}{dt} + \frac{dm_e}{dt}.$$
 (6)

For the bulk density of the grains produced by erosion, a value of 3000 kg/m³ is used, suitable for refractory silicate materials. A complete description of the method implemented for grain mass distribution can be found in the section Methods in Vida et al. (2023).²

Atmospheric Density Projection

We used a simulation by Cnossen (2022) with the Whole Atmosphere Community Climate Model – eXtended (WACCM-X) for the period 2015–2070 to estimate the future century-scale trend in the global mean mass density of air. This simulation followed the shared socio-economic pathway 2–4.5 (O'Neill et al., 2016), a "middle of the road" scenario, and also included realistic solar and geomagnetic activity variations, based on Matthes et al. (2017). In the thermosphere, the approximately 11-year solar cycle produces large variations in density, which far exceed the magnitude of the multi-decadal trend. To extract the century-scale trend in the global mean mass density, the model data was fitted to the following linear regression model:

$$\rho'_{\text{air}} = a + b \cdot F10.7a + c \cdot (F10.7a)^2 + d \cdot K_p + e \cdot \text{year},$$
(7)

where ρ'_{air} is the global mean mass density at a given altitude, F10.7a is the 81-day average of the F10.7 index of solar activity, K_p is the geomagnetic activity index,

and a, b, c, d, and e are coefficients to fit, with e corresponding to the trend.

While altitudes below the thermosphere are progressively less affected by solar and geomagnetic activity variations, the same formulation was used here, as the results for lower altitudes were not sensitive to omission/inclusion of the solar and geomagnetic activity terms. However, results in the thermosphere do vary somewhat depending on the exact time interval used, which is likely due to incomplete removal of solar activity effects. We therefore followed the approach of Chossen (2020, 2022) to use the average of the trends obtained for the 11 periods starting in January 2015 and ending in December 2060 to December 2070 (with each subsequent period being 12 months longer than the last). The global mean trend was used here, as mass density trends do not tend to vary much with location (e.g., Cnossen, 2020).

Simulating Winchcombe Fall With Another Atmosphere Density Profile

The semi-empirical model described in "Meteoroid Atmospheric Entry Model" section was successfully applied to reconstruct the fragmentation behavior and physical properties of many meteorite-dropping fireballs (Borovička et al., 2017, 2019, 2020; Borovička, Spurný, Šegon, et al., 2015; Brown et al., 2023; McMullan et al., 2024). This body of works shows that the fragmentation of chondritic meteorite-dropping meteoroids is primarily driven by mechanical stress, particularly due to aerodynamic loading as the meteoroid passes through the atmosphere. Fragmentation typically occurs when the dynamic pressure exerted by the atmosphere exceeds the cohesive strength of the meteoroid material. The dynamic pressure (P_{dyn}) can be expressed as:

$$P_{\rm dyn} = \Gamma v^2 \rho_{\rm air}.$$
 (8)

The Winchcombe fireball experienced an exceptionally low peak atmospheric dynamic pressure of approximately ~ 0.6 MPa, a result of its favorable entry conditions, allowing it to survive the atmospheric flight. Its structural fragility became evident when it underwent near-catastrophic fragmentation at a significantly lower pressure of only ~ 0.07 MPa.

To model the expected behavior of the Winchcombe meteoroid in a different atmosphere, we use the same initial conditions and physical properties while allowing the model to integrate the atmospheric flight, computing new light and deceleration curves. We enforce identical fragmentation events (type and mass loss) at the same dynamic pressure. This is

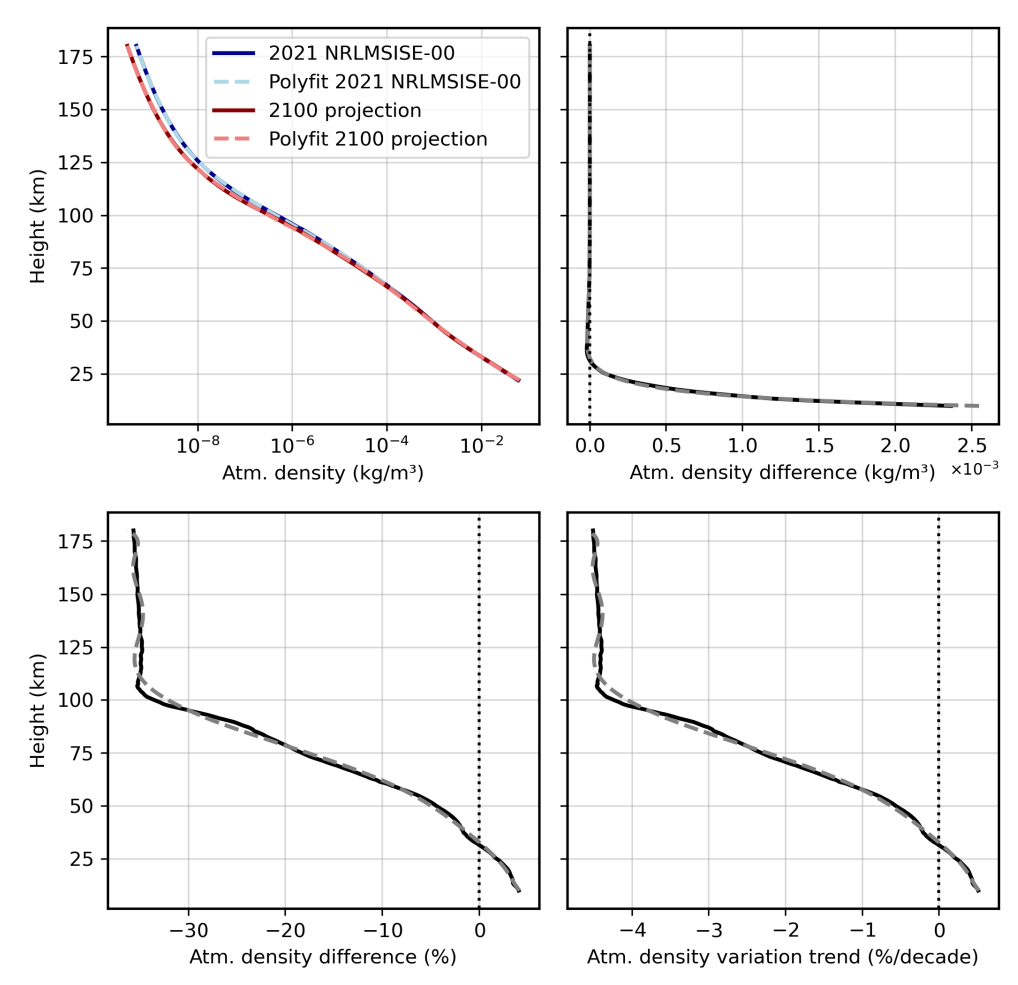


FIGURE 1. Top left: atmospheric density for 2021 (blue) and 2100 projection (red), with 11th-degree polynomial fits (lighter dashed). Top right: absolute difference (solid black) and its fit (dashed). Bottom left: percent difference (solid) and fit (dashed). Bottom right: trend in % per decade (solid) and fit (dashed). Differences are computed as projected (2100) minus reference (2021). (Color figure can be viewed at wileyonlinelibrary.com)

achieved by mapping the heights between different atmospheric density profiles.

In the original study of the Winchcombe fireball, a 7th degree polynomial was fitted to the logarithm of the atmospheric density profile to speed up the sampling of the atmospheric model at every integration step. In this analysis, we refine the approach employing an 11th degree polynomial to capture finer details. However, the differences between these approximations remain minimal.

To estimate a density profile for 2100, we apply the predicted atmospheric density trend to the year 2100 (Atmospheric Density Projection section) in the average trajectory location of the Winchcombe fireball (51 N, 2.6 W) at the same hour, day, and month. Throughout this study, we refer to 2021 as the observed event (the reference one), using the recorded atmospheric conditions, and 2100 as the projected scenario based on

the projected climate change. In this study, 2021 denotes the reference year with recorded atmospheric conditions on the event day, and 2100 denotes the projected climate-change scenario. All differences between model results are defined as projected (2100) minus reference (2021).

RESULTS

shows two profiles: the profile sampled from atmospheric density NRLMSISE-00 model appropriate for the time and location of the Winchcombe fireball (2021) and the projected profile for the year 2100, along with their respective polynomial fits. The polynomial approximation shows increasing relative residuals above 75 km. While this represents a larger relative deviation compared to lower altitudes, the absolute impact on

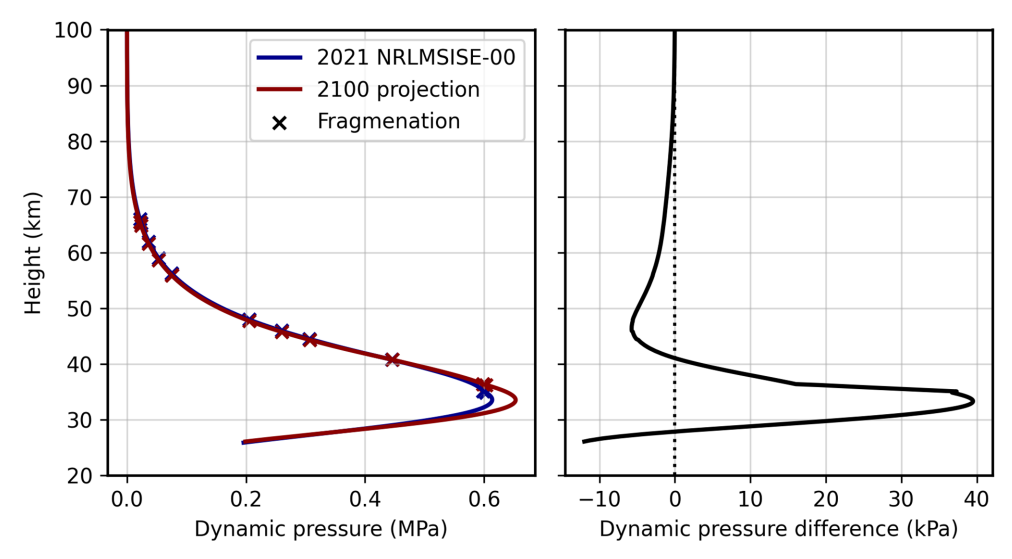


FIGURE 2. Dynamic pressure as a function of atmospheric height for the Winchcombe fireball (blue lines) and the simulated Winchcombe fall for the year 2100 considering climate change (red lines). The 11 fragmentation events are marked with crosses. The right panel represents the differences in dynamic pressure (black line). Difference is computed as projected (2100) minus reference (2021). (Color figure can be viewed at wileyonlinelibrary.com)

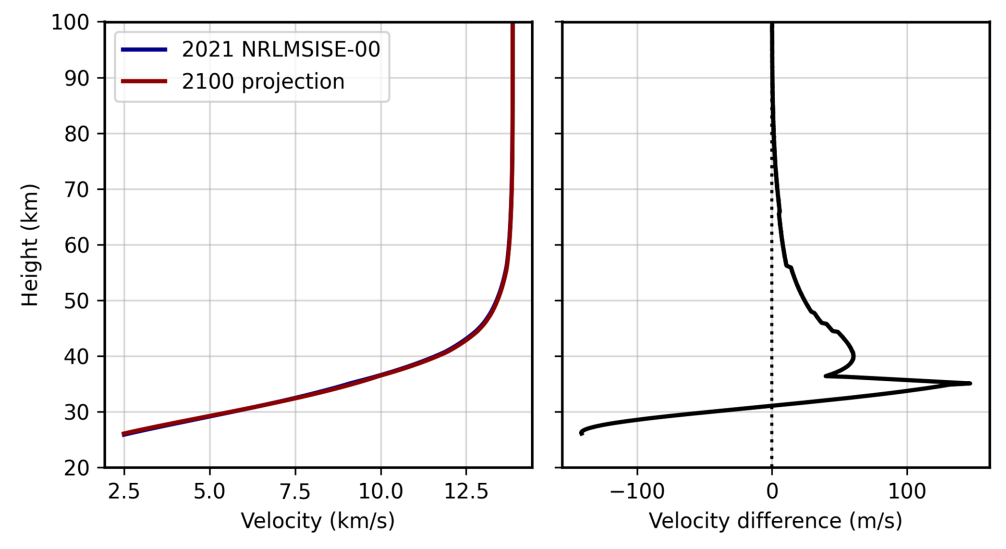


FIGURE 3. Velocity of the main fragment as a function of height for the Winchcombe fireball (blue line) and the simulated Winchcombe fall for the year 2100 considering climate change (red line). The right panel shows the velocity difference (black line). Difference is computed as projected (2100) minus reference (2021). (Color figure can be viewed at wileyonlinelibrary.com)

fragmentation and deceleration is minimal at such heights due to the low densities involved and the fact that luminosity is primarily generated by drag. Although the effects of climate change on atmospheric density are indeed more pronounced above $100\,\mathrm{km}$ due to the cumulative effect of atmospheric contraction below—projected to increase by $\sim\!35\%$ by 2100—this occurs at altitudes where atmospheric densities are low enough that the polynomial model retains sufficient accuracy to assess the entry behavior of meteoroids.

In addition, a trend reversal is observed, with the atmospheric density increasing below approximately 37 km. However, as shown in the top right panel of Figure 1, absolute differences in density are only noticeable below 25 km, and even at these lower altitudes, the variations remain relatively small (\sim 5%) and on par with diurnal and seasonal variations of up to 25% (Vida, Brown, et al., 2021).

Figure 2 presents the dynamic pressure as a function of atmospheric height for the Winchcombe fireball (2021)

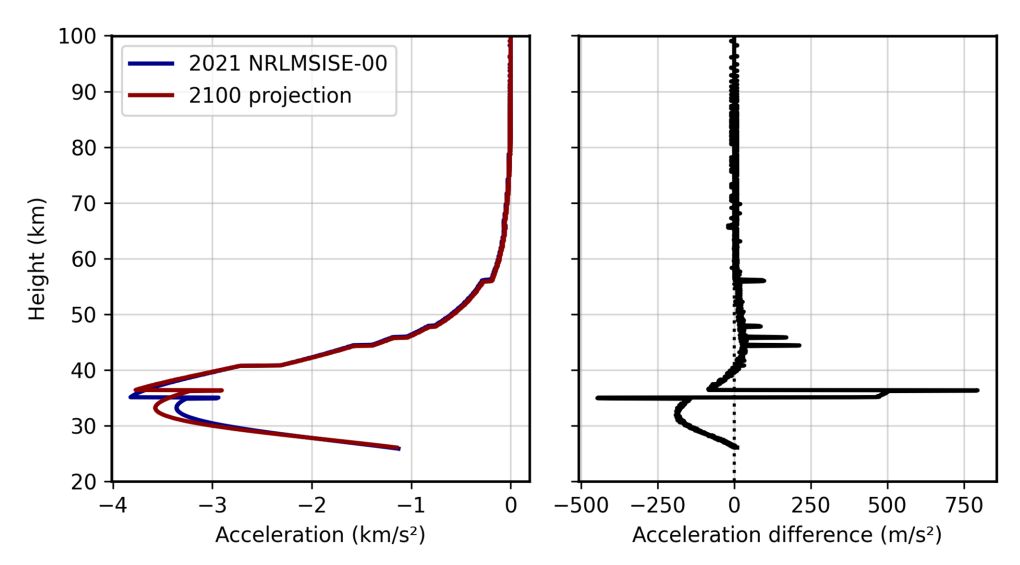


FIGURE 4. Acceleration of the main fragment as a function of height for the Winchcombe fireball (blue line) and the simulated Winchcombe fall for the year 2100 considering climate change (red line). The right panel shows the acceleration difference (black line). Difference is computed as projected (2100) minus reference (2021). (Color figure can be viewed at wileyonlinelibrary.com)

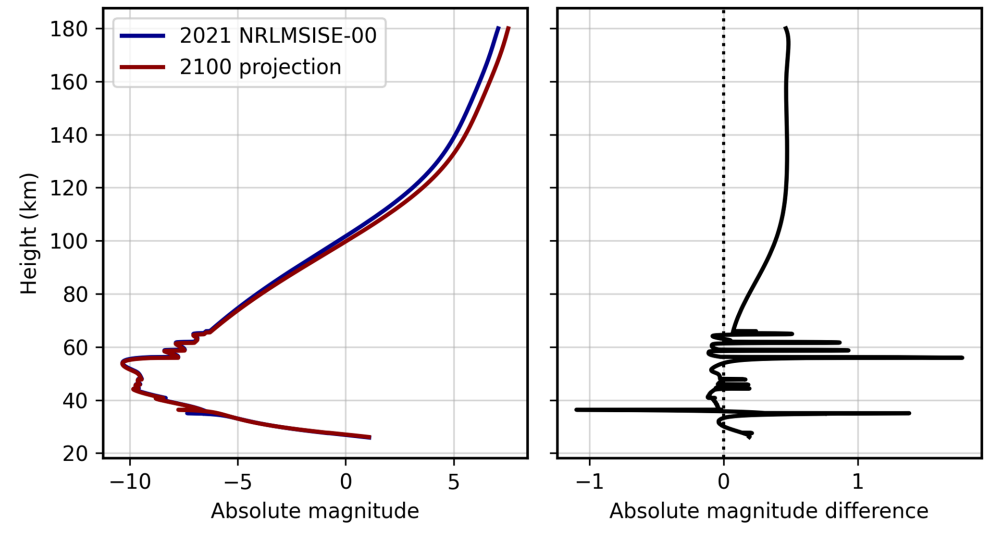


FIGURE 5. Absolute magnitude (brightness) of the main fragment as a function of height for the Winchcombe fireball (blue line) and the simulated Winchcombe fall for the year 2100 considering climate change (red line). The right panel shows the absolute magnitude difference (black line). Difference is computed as projected (2100) minus reference (2021). (Color figure can be viewed at wileyonlinelibrary.com)

and the simulated scenario for 2100 under climate change conditions. The right panel highlights the differences in dynamic pressure between the two scenarios. Above 41 km, the meteoroid experiences a lower dynamic pressure, with differences reaching up to 5 kPa. However, below 37 km, the dynamic pressure increases in the 2100 scenario and peaks at a maximum difference of 40 kPa (0.614 vs 0.653 MPa). Toward the final moments of the luminous flight, the dynamic pressure decreases again and remains 12 kPa lower in 2100 compared to 2021. This behavior reflects the interplay between atmospheric

density and deceleration. In the left panel of Figure 2, fragmentation events remain well aligned in terms of dynamic pressure but occur at different altitudes to ensure consistency (see Simulating Winchcombe Fall With Another Atmosphere Density Profile section).

Figure 3 shows the velocity of the main fragment as a function of height for the Winchcombe fireball (2021) and the simulated scenario for 2100. The velocity remains consistently higher throughout most of the trajectory in the 2100 scenario. This behavior is expected, as the atmosphere in 2100 is generally less dense, allowing the

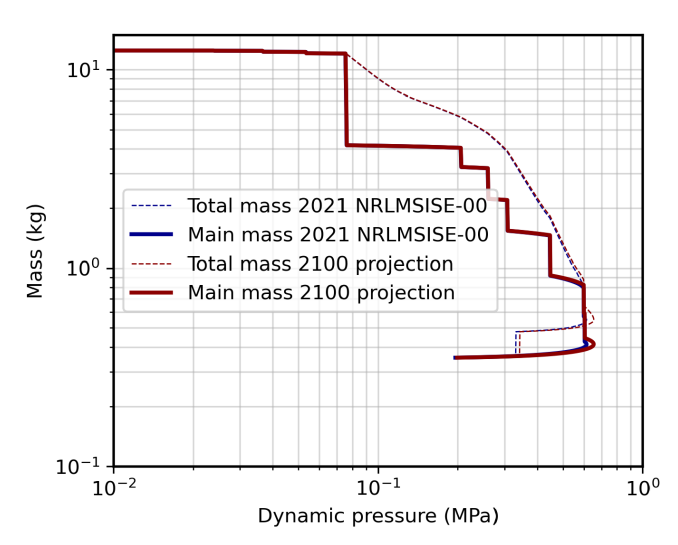


FIGURE 6. Mass of the main fragment (solid line) and the total mass (dashed line) versus the dynamic pressure for the Winchcombe fireball (blue lines) and the simulated Winchcombe fall for the year 2100 considering climate change (red lines). (Color figure can be viewed at wileyonlinelibrary.com)

meteoroid to experience lower deceleration at higher altitudes. However, once it reaches approximately 37 km, the increased atmospheric density in the 2100 scenario leads to a more rapid deceleration, as seen in Figure 4, reducing the velocity difference in the final phase of the luminous flight. The velocity difference varies between -147 and 141 m/s when comparing both scenarios.

Figure 5 presents the light curve of the main fragment as a function of height for the Winchcombe fireball (2021) and the simulated scenario for 2100 under climate change conditions. The absolute magnitude of a fireball is a normalized brightness at a fixed range of 100 km and without the effects of atmospheric extinction, with the brightness of the star Vega used as the zero point. Lower values indicate greater brightness, and a difference of one magnitude is equivalent to a brightness difference of 2.512×.

A clear difference is observed above 120 km, where the 2100 simulation is consistently fainter by approximately 0.5 magnitudes. This difference decreases at lower altitudes, with only brief peaks in brightness variation. These peaks are attributed to the different altitudes at which fragmentation events occur in each case. Despite these variations, the maximum brightness reached in both scenarios remains virtually the same, just brighter than magnitude –10. For example, a CCD camera with a limiting absolute magnitude of +3 would first detect the Winchcombe fireball 3 km lower in altitude in 2100.

Beginning with an initial mass of 12.5 kg, the meteoroid underwent only minor fragmentation above

60 km in altitude in both scenarios, at dynamic pressures not exceeding 0.06 MPa. For a complete representation of the atmospheric fragmentation history, Figure 6 shows the evolution of the main fragment mass (solid line) and the total mass (dashed line) as a function of dynamic pressure. The blue lines correspond to the Winchcombe fireball (2021), while the red lines depict the simulated fall for the year 2100 under climate change conditions.

In the 2100 simulation, the first fragmentation occurs 820 m lower than in the 2021 case, and the catastrophic fragmentation takes place 300 m lower. In contrast, the final luminous flight altitude is 190 m higher, and the meteorite mass is reduced by 0.13 g (-0.037%) compared to the 2021 scenario. In Table 1, we compile the fragmentation behavior modeled for the Winchcombe fireball (2021) and the simulated fall under the 2100 climate change scenario, including the final height and the surviving meteorite mass at the end of the ablation. It is reasonable to assume that for larger and stronger meteoroids, the impact of atmospheric density variations on meteorite survival would be even smaller.

CONCLUSIONS

We have investigated the potential impact of climate change on meteorite falls by modeling the atmospheric entry of the Winchcombe meteoroid under predicted conditions for the year 2100, assuming a moderate future emission scenario. The combination of high-quality observational data, including light and deceleration curves, together with detailed fragmentation modeling and the inherent fragility of the meteoroid, makes the Winchcombe event an ideal case study to evaluate the impact of atmospheric density variations on larger meteoroids that produce meteorites.

The analysis indicates that, while the projected 2100 atmosphere exhibits a systematic reduction in density at high altitudes, the overall atmospheric flight is only modestly affected. Under these conditions, a CCD camera with a limiting absolute magnitude of +3 would detect the Winchcombe fireball 3 km lower in altitude. The first fragmentation occurs 820 m lower, and the catastrophic fragmentation takes place 300 m lower, while the luminous flight ends 190 m higher. Furthermore, the surviving meteorite mass is reduced by approximately 0.1 g compared to the real case.

In contrast to small meteoroids, which completely ablate at higher altitudes and are therefore more strongly affected by changes in atmospheric density, larger and slower meteoroids do not experience significant alterations in their ablation process. Overall, these results suggest that century-scale changes in atmospheric density due to climate change have a moderate impact on bright fireballs and a limited effect on meteorite survival.

TABLE 1. Modeled fragmentation behavior for the Winchcombe fireball (2021) and the simulated Winchcombe fall considering climate change (2100).

Height (km)		Velocity (km/s)		P_{dyn} (MPa)			Mass loss (kg)		Meteorite (g)	
2021	2100	2021	2100	2021	2100	Frag.	2021	2100	2021	2100
65.30	64.85	13.80	13.80	0.024	0.024	EF	0.025	0.025	_	
62.00	61.60	13.77	13.78	0.037	0.037	EF	0.124	0.124	_	_
59.00	58.66	13.74	13.74	0.053	0.053	EF	0.184	0.184	_	_
56.25	55.94	13.69	13.69	0.075	0.075	EF	4.343	4.343	_	_
56.20	55.91	13.68	13.69	0.075	0.076	EF	3.551	3.552	_	_
48.00	47.76	13.23	13.24	0.205	0.206	EF	0.809	0.809	_	_
46.00	45.78	13.02	13.03	0.260	0.260	EF	0.957	0.957	_	_
44.50	44.36	12.79	12.81	0.307	0.307	EF	0.660	0.661	_	_
40.80	40.80	11.90	11.96	0.445	0.446	EF	0.539	0.541	1.12	1.05
35.10	36.40	9.10	9.93	0.598	0.599	D	0.222	0.231	_	_
34.90	36.26	9.00	9.88	0.603	0.604	$3 \times F$	0.142	0.148	3×117.67	3×117.65
25.89	26.08	_	_	_	_	_	_	_	354.12	353.99

Note: The last row represents the final height and mass of the main fragment at the end of ablation.

Abbreviations: D, dust ejection; EF, eroding fragment; F, single-body fragment.

Acknowledgments—EP-A acknowledges financial support from the LUMIO project funded by the Agenzia Spaziale Italiana (2024-6-HH.0). DV was supported in part by the NASA Meteoroid Environment Office under cooperative agreement 80NSSC24M0060. IC was supported by a Natural Environment Research Council (NERC) Independent Research Fellowship (NE/R015651/1). EF acknowledges the funding received by the Grant DeepCFD (Project No. PID2022-137899OB-I00) funded by MICIU/AEI/10.13039/501100011033 and by ERDF, EU. Open access publishing facilitated by Politecnico di Milano, as part of the Wiley - CRUI-CARE agreement.

Data Availability Statement—The data that support the findings of this study are available on request from the corresponding author. The data are not publicly available due to privacy or ethical restrictions.

Editorial Handling-Dr. Maria Gritsevich

Endnotes

REFERENCES

Binzel, R. P., DeMeo, F. E., Turtelboom, E. V., Bus, S. J., Tokunaga, A., Burbine, T. H., Lantz, C., et al. 2019. Compositional Distributions and Evolutionary Processes for the Near-Earth Object Population: Results from the MIT-Hawaii Near-Earth Object Spectroscopic Survey (MITHNEOS). *Icarus* 324: 41–76.

Borovička, J., Popova, O., and Spurný, P. 2019. The Maribo CM2 Meteorite Fall—Survival of Weak Material at High Entry Speed. *Meteoritics & Planetary Science* 54: 1024–41.

Borovička, J., Spurný, P., and Brown, P. 2015. Small Near-Earth Asteroids as a Source of Meteorites. In *Asteroids IV*, edited by P. Michel, F. E. DeMeo, and W. F. Bottke, 257–280. Tucson: The University of Arizona Press.

Borovička, J., Spurný, P., Grigore, V. I., and Svoreň, J. 2017. The January 7, 2015, Superbolide over Romania and Structural Diversity of Meter-Sized Asteroids. *Planetary and Space Science* 143: 147–158.

Borovička, J., Spurný, P., Šegon, D., Andreić, Ž., Kac, J., Korlević, K., Atanackov, J., et al. 2015. The Instrumentally Recorded Fall of the Križevci Meteorite, Croatia, February 4, 2011. *Meteoritics & Planetary Science* 50: 1244–59.

Borovička, J., Spurný, P., and Shrbený, L. 2020. Two Strengths of Ordinary Chondritic Meteoroids as Derived from their Atmospheric Fragmentation Modeling. *The Astronomical Journal* 160: 42.

Borovička, J., Tóth, J., Igaz, A., Spurný, P., Kalenda, P., Haloda, J., Svoreå, J., et al. 2013. The Košice Meteorite Fall: Atmospheric Trajectory, Fragmentation, and Orbit. *Meteoritics & Planetary Science* 48: 1757–79.

Brown, M., Lewis, H., Kavanagh, A., Cnossen, I., and Elvidge, S. 2024. Future Climate Change in the Thermosphere under Varying Solar Activity Conditions. *Journal of Geophysical Research, Space Physics* 129: e2024JA032659.

Brown, M. K., Lewis, H. G., Kavanagh, A. J., and Cnossen, I. 2021. Future Decreases in Thermospheric Neutral Density in Low Earth Orbit Due to Carbon Dioxide Emissions. *Journal of Geophysical Research: Atmospheres* 126: e2021JD034589.

Brown, P. G., Hildebrand, A. R., Zolensky, M. E., Grady, M., Clayton, R. N., Mayeda, T. K., Tagliaferri, E., et al. 2000. The Fall, Recovery, Orbit, and Composition of the Tagish Lake Meteorite: A New Type of Carbonaceous Chondrite. *Science* 290: 320–25.

¹ https://www.lpi.usra.edu/meteor/.

² The corresponding code implementation is openly available at https://github.com/wmpg/WesternMeteorPyLib.

- Brown, P. G., McCausland, P. J. A., Hildebrand, A. R., Hanton, L. T. J., Eckart, L. M., Busemann, H., Krietsch, D., et al. 2023. The Golden Meteorite Fall: Fireball Trajectory, Orbit, and Meteorite Characterization. *Meteoritics & Planetary Science* 58: 1773–1807.
- Brown, P. G., Revelle, D. O., Tagliaferri, E., and Hildebrand, A. R. 2002. An Entry Model for the Tagish Lake Fireball Using Seismic, Satellite and Infrasound Records. *Meteoritics & Planetary Science* 37: 661–675.
- Brož, M., Vernazza, P., Marsset, M., Binzel, R. P., DeMeo, F., Birlan, M., Colas, F., et al. 2024. Source Regions of Carbonaceous Meteorites and near-Earth Objects. *Astronomy & Astrophysics* 689: A183.
- Campbell-Burns, P., and Kacerek, R. 2014. The UK Meteor Observation Network. WGN, Journal of the International Meteor Organization 42: 139–144.
- Ceplecha, Z., Borovička, J., Elford, W. G., Revelle, D. O., Hawkes, R. L., Porubčan, V., and Šimek, M. 1998. Meteor Phenomena and Bodies. *Space Science Reviews* 84: 327–471.
- Clemesha, B., and Batista, P. 2006. The Quantification of Long-Term Atmospheric Change Via Meteor Ablation Height Measurements. *Journal of Atmospheric and Solar-Terrestrial Physics* 68: 1934–39.
- Cnossen, I. 2020. Analysis and Attribution of Climate Change in the Upper Atmosphere from 1950 to 2015 Simulated by WACCM-X. *Journal of Geophysical Research: Space Physics* 125: e2020JA028623.
- Cnossen, I. 2022. A Realistic Projection of Climate Change in the Upper Atmosphere into the 21st Century. *Geophysical Research Letters* 49: e2022GL100693.
- Cnossen, I., Emmert, J. T., Garcia, R. R., Elias, A. G., Mlynczak, M. G., and Zhang, S.-R. 2024. A Review of Global Long-Term Changes in the Mesosphere, Thermosphere and Ionosphere: A Starting Point for Inclusion in (Semi-) Empirical Models. Advances in Space Research 74: 5991–6011.
- Colas, F., Zanda, B., Bouley, S., Jeanne, S., Malgoyre, A.,
 Birlan, M., Blanpain, C., et al. 2020. FRIPON: A
 Worldwide Network to Track Incoming Meteoroids.
 Astronomy & Astrophysics 644: A53.
- Daly, L., McMullan, S., Rowe, J., Collins, G. S., Suttle, M., Chan, Q. H. S., Young, J. S., et al. 2020. The UK Fireball Alliance (UKFAll); Combining and Integrating the Diversity of UK Camera Networks to Aim to Recover the First UK Meteorite Fall for 30 Years. In European Planetary Science Congress, EPSC2020-705.
- Dawkins, E. C. M., Stober, G., Janches, D., Carrillo-Sánchez, J. D., Lieberman, R. S., Jacobi, C., Moffat-Griffin, T., et al. 2023. Solar Cycle and Long-Term Trends in the Observed Peak of the Meteor Altitude Distributions by Meteor Radars. Geophysical Research Letters 50: e2022GL101953.
- Devillepoix, H. A. R., Cupák, M., Bland, P. A., Sansom, E. K., Towner, M. C., Howie, R. M., Hartig, B. A. D., et al. 2020. A Global Fireball Observatory. *Planetary and Space Science* 191: 105036.
- Emmert, J. T. 2015. Altitude and Solar Activity Dependence of 1967–2005 Thermospheric Density Trends Derived from Orbital Drag. *Journal of Geophysical Research: Space Physics* 120: 2940–50.
- Gattacceca, J., MCCubbin, F. M., Grossman, J., Bouvier, A., Chabot, N. L., D'Orazio, M., Goodrich, C., et al. 2022. The Meteoritical Bulletin, No. 110. *Meteoritics & Planetary Science* 57: 2102–5.

- Hankey, M., Meisel, D., and Perlerin, V. 2020. The All-Sky-6 and Video Meteor Archive System of the AMS Ltd. In *International Meteor Conference*, edited by U. Pajer, J. Rendtel, M. Gyssens, and C. Verbeeck, 21–25. Germany: Bollmannsruh.
- Hromakina, T., Birlan, M., Barucci, M. A., Fulchignoni, M., Colas, F., Fornasier, S., Merlin, F., et al. 2021. Photometric Survey of 55 Near-Earth Asteroids. *Astronomy and Astrophysics* 656: A89.
- Ieva, S., Dotto, E., Mazzotta Epifani, E., Perna, D., Fanasca, C., Lazzarin, M., Bertini, I., et al. 2020. Extended Photometric Survey of Near-Earth Objects. Astronomy & Astrophysics 644: A23.
- Jacobi, C. 2014. Meteor Heights during the Recent Solar Minimum. Advances in Radio Science 12: 161–65.
- King, A. J., Daly, L., Rowe, J., Joy, K. H., Greenwood, R. C., Devillepoix, H. A. R., Suttle, M. D., et al. 2022. The Winchcombe Meteorite, a Unique and Pristine Witness from the Outer Solar System. Science Advances 8: eabq3925.
- Koschny, D., and Borovicka, J. 2017. Definitions of Terms in Meteor Astronomy. WGN, Journal of the International Meteor Organization 45: 91–92.
- Lima, L. M., Araújo, L. R., Alves, E. O., Batista, P. P., and Clemesha, B. R. 2015. Variations in Meteor Heights at 22.7° S during Solar Cycle 23. *Journal of Atmospheric and Solar-Terrestrial Physics* 133: 139–144.
- Lyytinen, E., and Gritsevich, M. 2016. Implications of the Atmospheric Density Profile in the Processing of Fireball Observations. *Planetary and Space Science* 120: 35–42.
- Manabe, S., and Wetherald, R. T. 1967. Thermal Equilibrium of the Atmosphere with a Given Distribution of Relative Humidity. *Journal of the Atmospheric Sciences* 24: 241–259.
- Manabe, S., and Wetherald, R. T. 1975. The Effects of Doubling the CO₂ Concentration on the Climate of a General Circulation Model. *Journal of the Atmospheric Sciences* 32: 3–15.
- Matthes, K., Funke, B., Andersson, M. E., Barnard, L., Beer, J., Charbonneau, P., Clilverd, M. A., et al. 2017. Solar Forcing for CMIP6 (v3.2). *Geoscientific Model Development* 10: 2247–2302.
- McMullan, S., Vida, D., Devillepoix, H. A. R., Rowe, J., Daly, L., King, A. J., Cupák, M., et al. 2024. The Winchcombe Fireball—That Lucky Survivor. *Meteoritics and Planetary Science* 59: 927–947.
- O'Neill, B. C., Tebaldi, C., van Vuuren, D. P., Eyring, V., Friedlingstein, P., Hurtt, G., Knutti, R., et al. 2016. The Scenario Model Intercomparison Project (Scenario MIP) for CMIP6. *Geoscientific Model Development* 9: 3461–82.
- Picone, J. M., Hedin, A. E., Drob, D. P., and Aikin, A. C. 2002. NRLMSISE-00 Empirical Model of the Atmosphere: Statistical Comparisons and Scientific Issues. *Journal of Geophysical Research, Space Physics* 107(A12): 1468.
- Roble, R. G., and Dickinson, R. E. 1989. How Will Changes in Carbon Dioxide and Methane Modify the Mean Structure of the Mesosphere and Thermosphere? *Geophysical Research Letters* 16: 1441–44.
- Russell, S. S., King, A. J., Bates, H. C., Almeida, N. V., Greenwood, R. C., Daly, L., Joy, K. H., et al. 2024. Recovery and Curation of the Winchcombe (CM2) Meteorite. *Meteoritics & Planetary Science* 59: 973–987.
- Shober, P. M., Devillepoix, H. A. R., Vaubaillon, J., Anghel, S., Deam, S. E., Sansom, E. K., Colas, F., Zanda, B.,

19455100, 2025, 10, Downloaded from https://onlinelibrary.wiley.com/doi/10.1111/maps.70046 by British Antarctic Survey, Wiley Online Library on [20/10/2025]. See the Terms conditions) on Wiley Online Library for rules of use; OA articles are governed by the applicable Creative Commons Licensa

- Vernazza, P., and Bland, P. 2025. Perihelion History and Atmospheric Survival as Primary Drivers of the earth's Meteorite Record. *Nature Astronomy* 9: 799–812.
- Stewart, W., Pratt, A. R., and Entwisle, L. 2013. NEMETODE: The Network for Meteor Triangulation and Orbit Determination. System Overview and Initial Results from a UK Video Meteor Network. WGN, Journal of the International Meteor Organization 41: 84–91.
- Stober, G., Jacobi, C., Matthias, V., Hoffmann, P., and Gerding, M. 2012. Neutral Air Density Variations during Strong Planetary Wave Activity in the Mesopause Region Derived from Meteor Radar Observations. *Journal of Atmospheric and Solar-Terrestrial Physics* 74: 55–63.
- Stober, G., Matthias, V., Brown, P., and Chau, J. L. 2014. Neutral Density Variation from Specular Meteor Echo Observations Spanning One Solar Cycle. *Geophysical Research Letters* 41: 6919–25.
- Suttle, M. D., Daly, L., Jones, R. H., Jenkins, L., van Ginneken, M., Mitchell, J. T., Bridges, J. C., et al. 2024. The Winchcombe Meteorite—A Regolith Breccia from a Rubble Pile CM Chondrite Asteroid. *Meteoritics & Planetary Science* 59: 1043–67.

- Venkat Ratnam, M., Teja, A., Pramitha, M., Eswaraiah, S., and Vijaya Bhaskara Rao, S. 2025. Climatology of Meteor Echoes and Mean Winds in the Mlt Region Revealed by Svu Meteor Radar over Tirupati (13.63on, 79.4oe): Long-Term Trends. Advances in Space Research 75: 4768–75.
- Vida, D., Brown, P. G., Campbell-Brown, M., Weryk, R. J., Stober, G., and McCormack, J. P. 2021. High Precision Meteor Observations with the Canadian Automated Meteor Observatory: Data Reduction Pipeline and Application to Meteoroid Mechanical Strength Measurements. *Icarus* 354: 114097.
- Vida, D., Brown, P. G., Devillepoix, H. A. R., Wiegert, P., Moser, D. E., Matlovič, P., Herd, C. D. K., et al. 2023. Direct Measurement of Decimetre-Sized Rocky Material in the Oort Cloud. *Nature Astronomy* 7: 318–329.
- Vida, D., Šegon, D., Gural, P. S., Brown, P. G., McIntyre, M. J.
 M., Dijkema, T. J., Pavletić, L., et al. 2021. The Global Meteor Network – Methodology and First Results. *Monthly Notices of the Royal Astronomical Society* 506: 5046–74.
- Weng, L., Lei, J., Zhong, J., Dou, X., and Fang, H. 2020. A Machine-Learning Approach to Derive Long-Term Trends of Thermospheric Density. *Geophysical Research Letters* 47: e2020GL087140.